

Thermal decomposition kinetics of electrospun azidodeoxy cellulose nitrate and polyurethane nanofibers

Seied Mahdi Pourmortazavi · Minoos Sadri · Mehdi Rahimi-Nasrabadi ·
Mojtaba Shamsipur · Yousef Jabbarzade · Morteza Shafaghi Khalaki ·
Morteza Abdollahi · Zahra Shariatinia · Iraj Kohsari · Seyed Mahdi Atifeh

Received: 3 March 2014 / Accepted: 1 August 2014 / Published online: 28 August 2014
© Akadémiai Kiadó, Budapest, Hungary 2014

Abstract Thermal behaviors of electrospun polymer nanofibers including azidodeoxy cellulose nitrate (ACN) and polyurethane (PU) were studied by thermal analysis techniques i.e., differential scanning calorimetry (DSC) and thermogravimetry (TG). Thermoanalytical results revealed that main thermal degradation for the ACN nanofibers occurs during three individual steps at the temperature range of 160–500 °C. Similarly, PU nanofibers decompose completely during three steps at the temperature range of 190–460 °C. However, nanofibers of ACN and PU have lower thermal stabilities in comparison with their bulk form. Thermal decomposition kinetic of the

nanofibers was studied by non-isothermal DSC at different heating rates. Meanwhile, thermal decomposition kinetic of nanofibers was studied by non-isothermal DSC at different heating rates.

Keywords Thermal stability · Nanofibers decomposition · Kinetic parameters · Electrospun polymers · Azidodeoxy cellulose nitrate · Polyurethane

Introduction

Polymeric materials i.e., azidodeoxy cellulose nitrate (ACN) and polyurethane are used as binder to adhere solid particles to each other in order to formulate fuel and oxidizer in composite explosives or composite propellants [1–4]. Nitrocellulose with high nitrogen-content is one of the most widely used energetic polymers. Azidodeoxy cellulose nitrate (ACN) with the chemical structure shown in Fig. 1a is one of the cellulose nitrate derivatives. The use of ACN as an energetic binder is under investigation during recent years [3, 4].

Polyurethanes are a main class of synthetic elastomers. The polymer group of polyurethanes includes all polymers that contain urethane i.e., urea or other isocyanate derived groups. The commonly used reagents for the partitioned polyurethanes are including a diisocyanate, a polyol, and an extender. The polyurethanes can be considered as multi-block copolymers, consisting of a hard and a soft block section. This group of polymers forms a versatile class of polymers, which are used in a various range of applications such as elastomers, foams, coatings, fibers, and biomedical materials [5–9].

Recently, nanofibers have obtained the attention of researchers due to their remarkable nano-structure

S. M. Pourmortazavi (✉) · Y. Jabbarzade · M. Abdollahi
Faculty of Material and Manufacturing Technologies, Malek
Ashtar University of Technology, P.O.Box 16765-3454, Tehran,
Iran
e-mail: pourmortazavi@yahoo.com

M. Sadri
Faculty of Bioscience Technologies, Malek Ashtar University of
Technology, Tehran, Iran

M. Rahimi-Nasrabadi
Nano Science Center, Imam Hossein University, Tehran, Iran

M. Shamsipur
Department of Chemistry, Razi University, Kermanshah, Iran

M. S. Khalaki
Department of Medicinal Chemistry, School of Pharmacy,
Shahid Beheshti University of Medical Sciences, Tehran, Iran

Z. Shariatinia · I. Kohsari
Department of Chemistry, Amir Kabir University of
Technology, Tehran, Iran

S. M. Atifeh
Department of Chemistry, Imam Hossein University, Tehran,
Iran

characteristics i.e., high surface area, small pore size, and the possibility of their producing three dimensional structures that enable the development of advanced materials with sophisticated applications [10–12]. However, thermal stability and decomposition kinetic of nanofibers may be different from micron-sized particles of a same polymer. Meanwhile, the particle size of materials could influences on the systems performance especially in propellants, pyrotechnics, and explosives formulations [1, 2]. Therefore, investigation on the thermal stability of nanofibers (before their using in various formulations and compositions) is essential in order to obtain safety and stability information for handling, storage, and usage of compositions containing nanofibers. Thermal analysis techniques i.e., TG, DSC, and DTA are useful methods for empirically understanding thermal properties of the polymers [13–20].

In this work, thermal stability of two polymers, which commonly used as binder in energetic compositions, including ACN and PU were investigated by means of simultaneous thermogravimetry–differential scanning calorimetry (TG/DSC). Effect of polymer particle size on thermal stability was studied using two different samples including electrospun nanofibers and micron-sized particles as foam shape material. Also, in this study, an attempt has been made to determine thermokinetic parameters on non-isothermal decomposition of the investigated electrospun nanofibers. To the best our knowledge, various data are available on thermal behaviors and decomposition kinetics of ACN [1] and PU in bulk form [21–23]. But, there is no report on the thermal

behavior and decomposition of ACN and polyurethane nanofibers.

Experimental

All chemical reagents, i.e., 4,4'-methylene bis (phenyl isocyanate), polycaprolactone diol (99 %) and 1,4-butanediol, and cellulose were purchased from Aldrich Company. The other chemicals, i.e., tetrahydrofuran, N,N- dimethyl formamide, sodium azide, and tetrachloroethylene and nitric acid, were from Merck (Darmstadt Germany) or Fluka (Buchs, Switzerland).

The investigated polymer materials (ACN and PU) were synthesized in chemistry laboratory. ACN polymer was synthesized as proposed by Ref. [24]. The polyether-polyurethane (PU) was prepared as shown in Fig. 1b, by reacting 4,4'-methylene bis (phenyl isocyanate) with polycaprolactone diol (99 %) and 1,4-butanediol as chain extending agent. The ratio of 1,4-butanediol to isocyanate and polycaprolactone was 5:1:1 [25]. The prepared polymers were characterized by NMR, FT-IR, and gel permeation chromatography techniques. NMR spectrum of the polymer in (D₆) DMSO, TMS was recorded on a Bruker 400 spectrometer. The IR spectrum of the PU sample was obtained on a FT-IR spectrophotometer (Perkin-Elmer 1600) using the KBr coins. The molecular weight of the PU sample was determined using gel permeation chromatography (Young Lin SP910D solvent delivery pumo, RI 750F refractive index detector).

Fig. 1 a Chemical structure of ACN; b synthesis reaction of PU

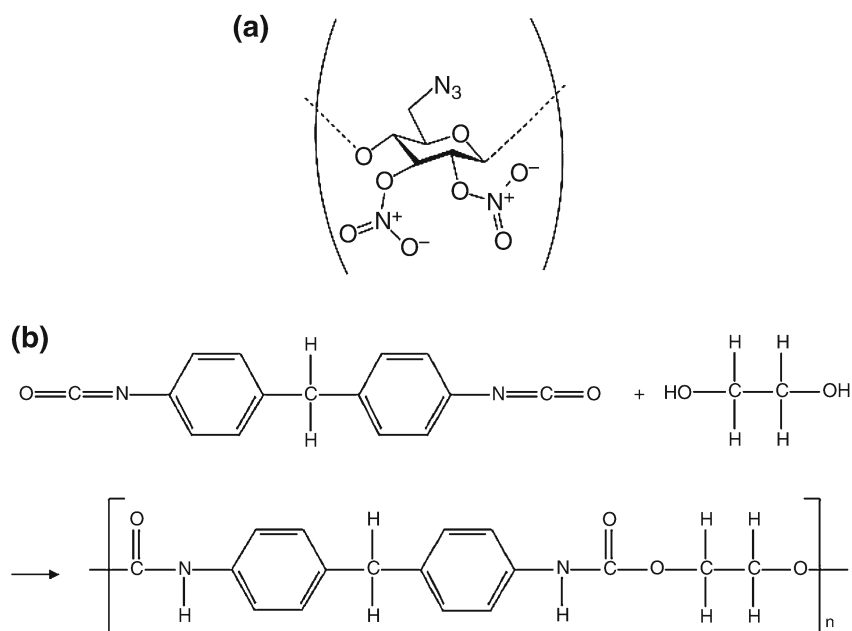
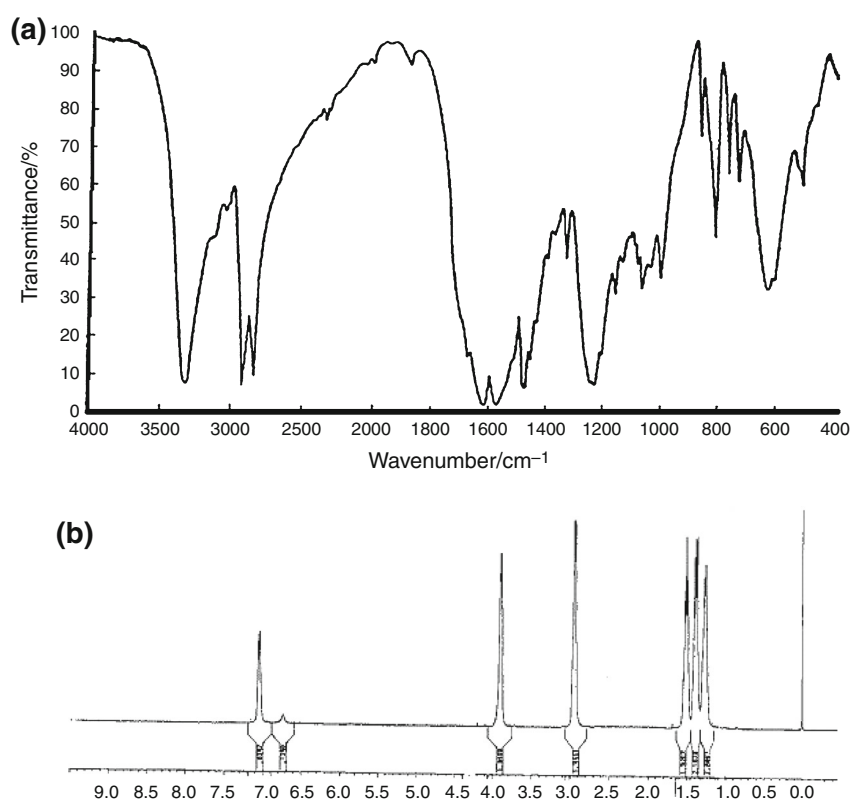


Fig. 2 Spectra of the synthesized PU polymer
a FT-IR spectrum and
b H-NMR spectrum



Electrospinning process was applied in order to generate polymers nanofibers. The PU and ACN solutions were prepared by dissolving their bulk materials in a mixture of solvents including 60 % THF and 40 % formaldehyde. The PU and ACN concentrations were 10 % (W/V, with respect to solvent). The prepared spinning solutions were immediately loaded into a plastic syringe with a needle inner diameter of 0.9 mm, while the syringe was fixed horizontally on a homemade syringe pump. The solutions were spun onto a grounded collector wrapped with aluminum foil. During the electrospinning process, the potential of 17 kV was attached to the needle using a high-voltage power supply. The distance between the needle tip and the collecting was 15 cm.

Thermogravimetric analysis (TG) and differential scanning calorimetry (DSC) were carried out by a Stanton Redcroft, STA-780 series. TG/DSC experiments were carried out in an alumina crucible, under heating rate of $10\text{ }^{\circ}\text{C min}^{-1}$ in a temperature range of 30–900 $^{\circ}\text{C}$. The purged gas was nitrogen with the flow rate of 50 mL min^{-1} . The used sample mass was about 3.0 mg.

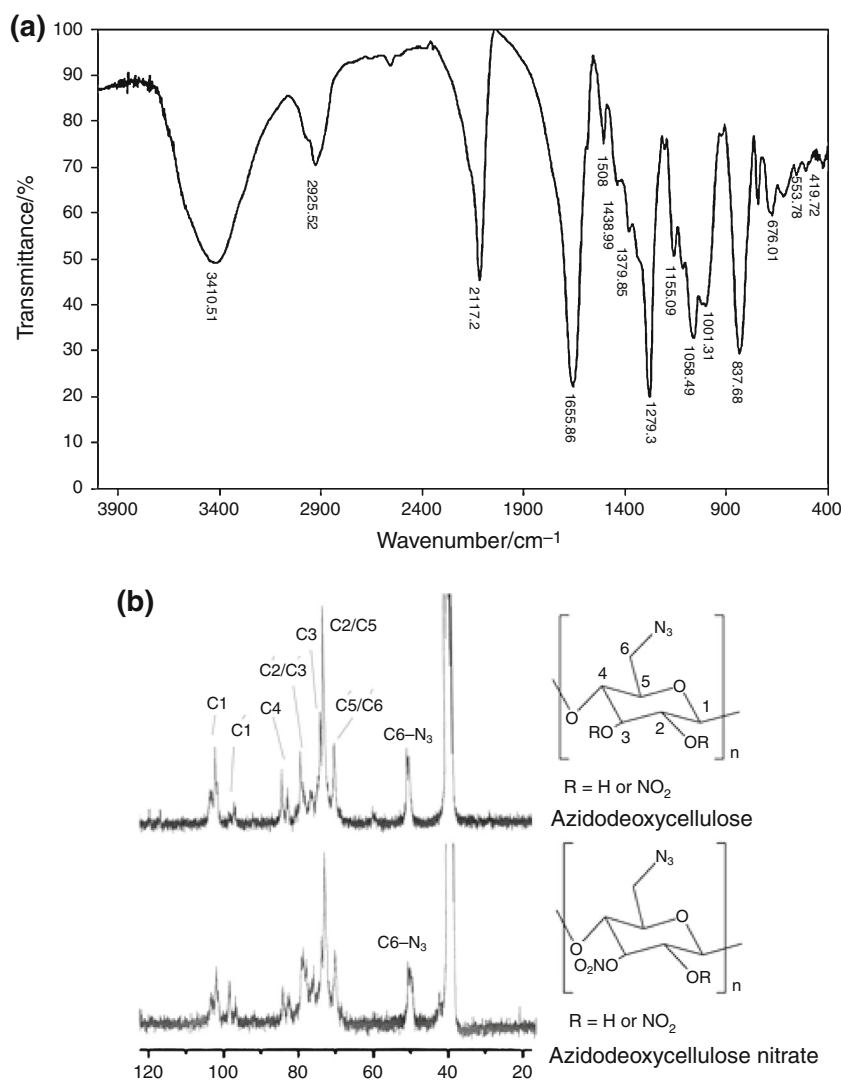
Thermokinetic and thermodynamic parameters correspond to the thermal decomposition of ACN and PU nanofibers were studied by non-isothermal DSC at different heating rates. DSC curves for decomposition of both polymers nanofibers at different heating rates (i.e., 5, 10, 15, and $20\text{ }^{\circ}\text{C min}^{-1}$) were obtained.

Results and discussion

Characterization of synthesized polymers

The synthesized polymer samples were characterized to determine the chemical composition and structure by NMR, FT-IR, and gel chromatography techniques. Figure 2a shows the FT-IR spectrum of the PU sample. The typical functional groups of the PU are shown in the spectrum. The N–H group absorbs at 1,545, 3,320, and $2,040\text{ cm}^{-1}$. The bands at $3,320\text{ cm}^{-1}$ and $2,040\text{ cm}^{-1}$ correspond to the non-bonded and bonded NH groups, respectively. The peaks at 1,687 and $1,545\text{ cm}^{-1}$ belong to the bonded and non-bonded carbonyl groups, respectively. Meanwhile, the strong peak appeared at $1,227\text{ cm}^{-1}$ corresponds to the C–O group adjacent to carbonyl group. Figure 2b presents the H-NMR spectrum of the PU. As seen in this figure, $\delta = 7.1$ and 6.7 ppm correspond to the hydrogen in NH, $\delta = 3.9$ ppm for (2H in CH_2O), 2.96 ppm (2H in CH_2N), 1.48 ppm (2H in $\text{CH}_2\text{CH}_2\text{O}$), and 1.40 ppm (2H in $\text{CH}_2\text{CH}_2\text{N}$). The other CH_2 group gives peak at 1.24 ppm. Furthermore, the gel permeation chromatography results were used to calculate the polydispersity and molecular weight of the sample relative to the polystyrene standard. The results showed that the synthesized PU has a molecular weight of 98,000 and polydispersity index (PDI) of 2.1. Figure 3a shows the FT-IR spectrum of the

Fig. 3 Spectra of the synthesized ACN polymer
a FT-IR spectrum and
b C-NMR spectrum



synthesized ACN. The typical functional groups correspond to the ACN could be observed in the spectrum. The asymmetric and symmetric bands, respectively, at 1,655 and 1,279 cm^{-1} are attributed to the O-NO₂ group. The vibration band at 837 cm^{-1} corresponds to the C-O-NO₂ group. The absorption peak at 2,117 cm^{-1} belongs to the azide group. Meanwhile, Fig. 3b presents the C-NMR spectrum of the synthesized ACN. As seen in the spectrum, the appeared peak at 50 ppm corresponds to the bonding of azide group to the C6, while the other peaks are specified in the figure. Furthermore, the gel permeation chromatography results were used to calculate the DP_n (degree of polymerization) of the ACN sample. The results showed that the synthesized ACN has a DP_n of 65.

Figure 4 shows SEM images of the prepared nanofibers. Figure 4a presents the SEM image of PU nanofibers prepared via electrospinning process. As seen in this figure, the PU nanofibers have an average diameter about 85 nm. On

the other hand, Fig. 4b shows the SEM image corresponds to the electrospun ACN nanofibers. As seen in this figure, ACN nanofibers have an average diameter about 70 nm. The prepared PU and ACN nanofibers were used to study their thermal stabilities and decomposition kinetics.

Thermal behavior of polymers samples

TG/DSC curves for PU samples are shown in Fig. 5. As shown in Fig. 5a, DSC curve for PU nanofibers sample shows three endothermic phenomena with minimum peak temperatures of 179.8, 341.7, and 424.2 °C. These results are compatible with TG curve of the PU nanofibers sample which shows three mass loss steps. At the first step, PU nanofibers undergo an endothermic phenomenon at about 179.8 °C due to the initiation of decomposition process. TG curve proves this result and presents approximately 5 % mass loss for this phenomenon. Also, DSC curve of PU

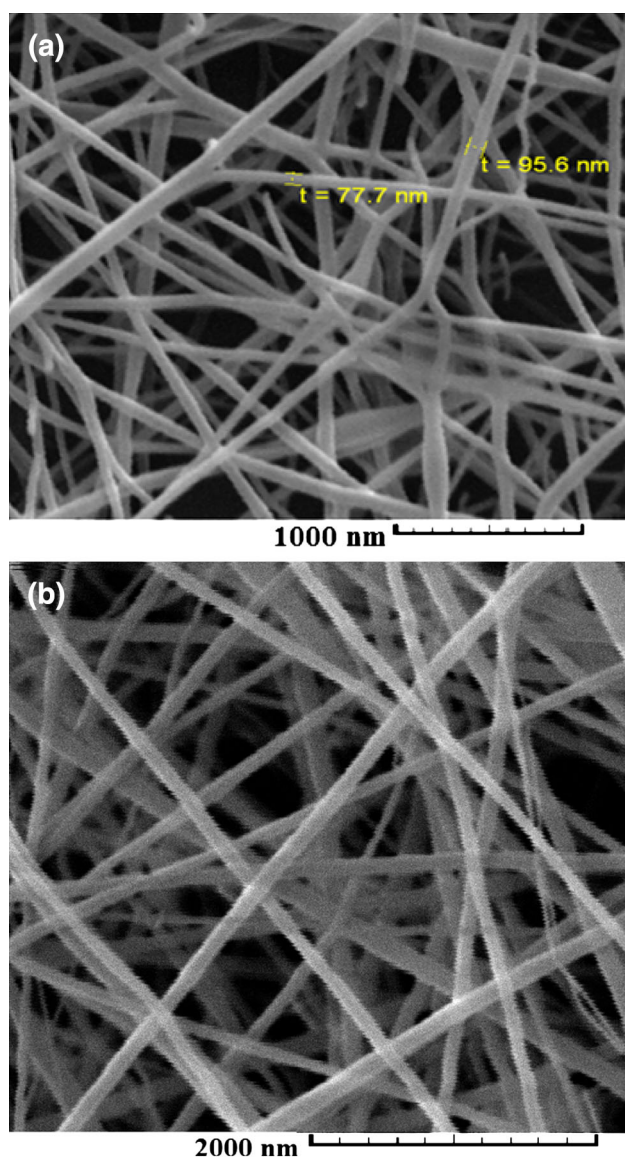


Fig. 4 SEM Images of Investigated Nanofibers: **a** PU and **b** ACN

nanofibers at higher temperatures present two other endothermic events at temperature range of 310–360 °C and 400–450 °C. The observed mass loss corresponds to the first temperature range was about 25 %, while the mass loss value for the second temperature range was approximately 63 %. These results show that thermal decomposition of the PU nanofibers started at about 170 °C along with 5 % mass loss that is probably due to the releasing the cyanide group from the backbone of the polymer followed by decomposing of polymer chain and consequently complete decomposition of PU nanofibers in the end of third step.

Figure 5b presents TG/DSC curves for PU in the bulk form. Thermal behavior of this sample is similar to the nanofibers sample. However, in the DSC curve, three endothermic peaks were observed with minimum at the

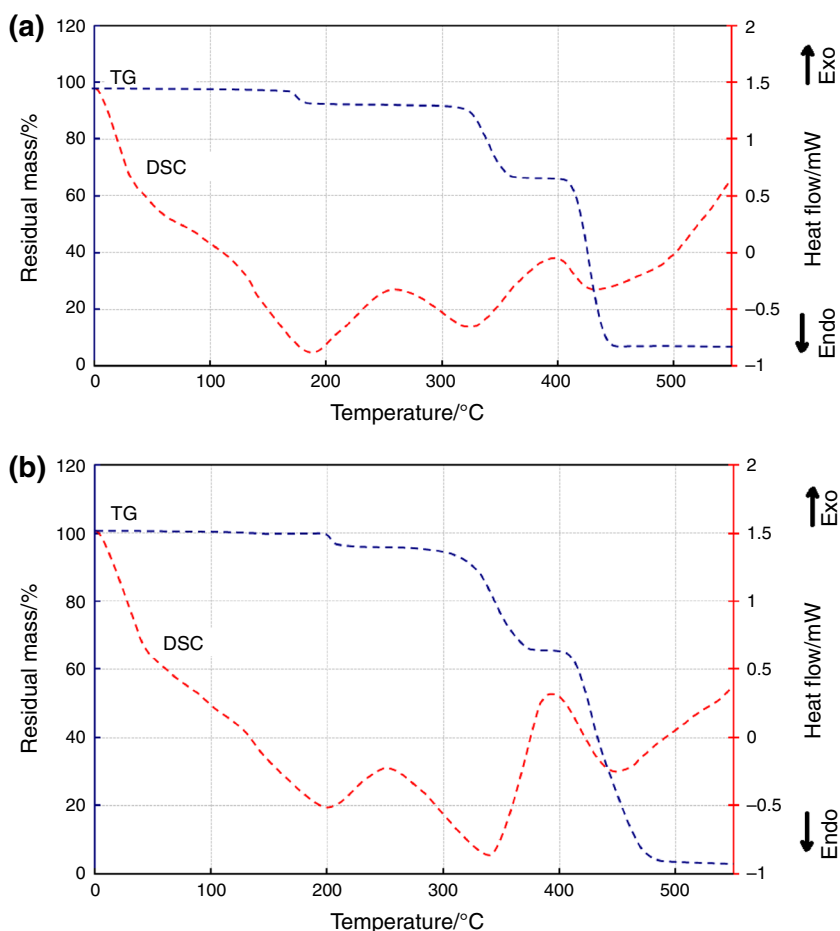
temperatures of 200.0, 344.7, and 450.2 °C. Here, again the first peak originates from starting thermal decomposition of the PU (at 192 °C), and probably realizing the functional group of the polymer followed by that of decomposition the backbone of the polymer at higher temperatures (344.7 and 450.2 °C). The results of TG for PU sample in the form of bulk material showed that the major endothermic decomposition is occurred around 350 °C. However, TG curve of this sample showed that the main decomposition of the compound was started at about 200 °C, and the decomposition was not completed until temperature of 490 °C. Previous studies [26] suggested that the loss of CN group occurs at the temperature range of 200–250 °C due to the decomposition of PU. Thermal behaviors of the PU samples were compared, and the results revealed that nanofibers of PU decompose endothermally during three main steps, and the mass loss in the first step is only about (4.3 %). However, bulk PU sample is decomposed endothermally during three main steps but its first mass losses (7.2 %) in the temperature range of 200–250 °C is more considerable (7.7 %).

The simultaneous TG/DSC curves of the ACN nanofibers are shown in Fig. 6a. No thermal event was observed prior to the decomposition of this energetic polymer. The TG curve exhibits a complete mass loss in the temperature range of 165–480 °C. This mass loss occurs during three individual steps. The results of TG/DSC and chemical structure of the polymer shown in Fig. 1a suggested that thermal decomposition of the polymer is started by elimination of the nitro group ($\Delta m_1 = 5$ %), and consequent further destruction of structure of the compound at the second step ($\Delta m_2 = 28$ %) which is followed by third step of decomposition reaction ($\Delta m_3 = 24$ %) [27]. TG/DSC curves of the bulk sample showed a similar trend. However, as seen in Fig. 6b, the main decomposition of the polymer was started at about 180 °C, and the decomposition was not completed until temperature of 550 °C. Comparison thermal behaviors of the ACN samples revealed that ACN in the bulk form is decomposed endothermally in the temperature range of 160–460 °C, while ACN nanofibers decompose at the lower temperature of about 180–550 °C. Table 1 summarizes the experimental results of TG/DSC analysis for both studied nanofibers and micro-particles of PU and ACN polymers.

Decomposition kinetic studies by DSC

Figure 7 presents DSC curves for decomposition of both polymers nanofibers at different heating rates (i.e., 5, 10, 15, and 20 °C min⁻¹). As seen in the figure, by increasing the heating rate, decomposition peaks of the ACN nanofibers and PU nanofibers were shifted to higher temperatures. These shifts were used to evaluate thermokinetic

Fig. 5 TG/DSC curves for polyurethane samples: **a** nanofibers and **b** micron-sized particles; sample mass 3.0 mg; heating rate $10\text{ }^{\circ}\text{C min}^{-1}$; nitrogen atmosphere



parameters of decomposition. ASTM E698 [28] as a well-known kinetic method was applied for prediction the Arrhenius parameters of ACN and PU nanofibers thermal decomposition. Therefore, the values of $\ln(\beta T_m^{-2})$ against $1/T_m$ were plotted, when β and T_m are DSC heating rate ($^{\circ}\text{C min}^{-1}$) and maximum DSC peak temperature, respectively. Table 2 shows the maximum peak temperature (T_m) correspond to the decomposition of each polymer at various heating rates (β) which are used to evaluate thermokinetic parameters via ASTM E698 method.

The plot of $\ln(\beta T_m^{-2})$ against $1/T_m$ resulted in the straight lines for both nanofibers ($r = 0.998$ for PU) and $r = 0.999$ for ACN), which indicated that the mechanism of thermal decomposition of these nanofibers undergoes no variation at various heating rates [29, 30]. The obtained slopes from these lines ($-E_a/R$) were used to calculate activation energy of each polymer nanofiber decomposition. Thereafter, the obtained values of activation energies for nanofibers samples were used for computing the logarithm of pre-exponential factor, $\log(Z/S^{-1})$, using the following expression as recommended by ASTM E698:

$$Z = \beta (E_a/RT_m^2) \exp(E_a/RT_m). \quad (1)$$

The ASTM method resulted in the values of the activation energy and frequency factors for both nanofibers samples. The results are presented in Table 3 for PU nanofibers and ACN nanofibers. Meanwhile, the values of activation energy (E_a) for these nanofibers samples were calculated by Starink method [31]. In this method, activation energy is determined by plotting of the $\ln(\beta T_m^{-1.92})$ versus the inverse of the temperature at the maximum reaction rate in the experiments with a constant heating rate. This method could be used for determination of the activation energy without a precise knowledge of the reaction mechanism, via following equation:

$$\ln(\beta/T_m^{1.92}) + 1.0008 E_a/RT_m = C. \quad (2)$$

The plotting of $\ln(\beta/T_m^{1.92})$ versus reciprocal of the absolute peak temperature for both nanofibers samples resulted in the straight lines (with $r = 0.998$ for PU and $r = 0.999$ for ACN). The obtained slopes from these lines were used to compute the values of the activation energy for each nanofibers sample. Then, the values of frequency factor (Z) correspond to the thermal decomposition reaction of each nanofibers samples were calculated by Eq. (1)

Fig. 6 TG/DSC curves for ACN samples: **a** nanofibers and **b** micron-sized particles; sample mass 3.0 mg; heating rate 10 °C min⁻¹; nitrogen atmosphere

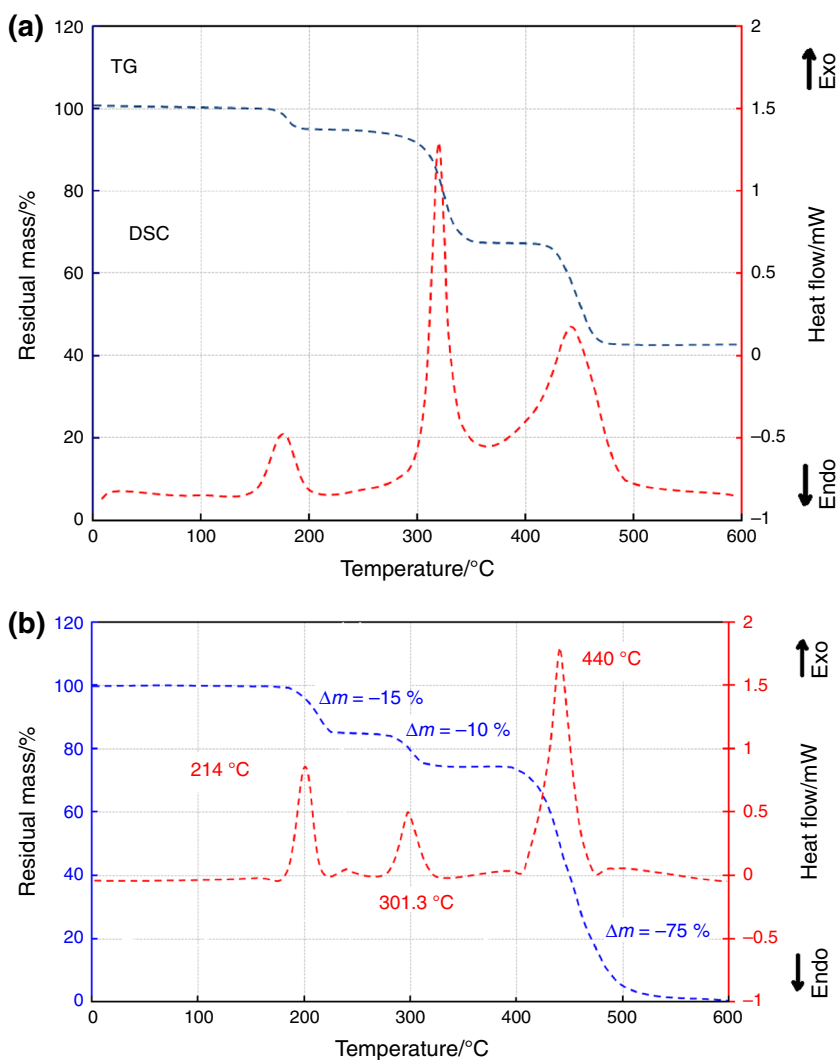


Table 1 Summary of thermoanalytical results of the investigated polymer samples

Compound	Form	First Step of Decomposition/ °C	T*/°C	Total Mass Loss/%
PU	Nanofibers	179.8	155–445	93
	Bulk	203.5	167–550	97
ACN	Nanofibers	168.8	160–460	58
	Bulk	214.0	180–550	95

T* is the temperature range when there is fall in a sample’s mass

[29, 30]. Table 3 presents the calculated Arrhenius data for PU and ACN nanofibers.

Thermodynamic parameters for thermal activation of the decomposition reaction of these nanofibers could be estimated using the following equations and thermokinetic data calculated by ASTM and Starink methods. Therefore, the values of activation entropy (ΔS^\ddagger), activation enthalpy

(ΔH^\ddagger), and free energy of activation (ΔG^\ddagger) were estimated via the Eqs. (3–5) [32–34]:

$$A \exp \frac{-E}{RT} = v \exp \frac{-\Delta G^\ddagger}{RT}, \tag{3}$$

$$\Delta H^\ddagger = E - RT, \tag{4}$$

$$\Delta G^\ddagger = \Delta H^\ddagger - T\Delta S^\ddagger. \tag{5}$$

In the Eq. 3, $v = K_B T/h$ (where h and K_B are Plank and Boltzmann constants, respectively). The calculated values of thermodynamic parameters for the PU and ACN nanofibers are shown in Table 3. Comparison of these thermodynamic parameters shows that ΔS^\ddagger for the ACN nanofibers is lower than PU nanofibers, which means the corresponding activated complex has a higher degree of arrangement (higher entropy) than its initial state, while this trend for the PU nanofibers was reversed. Based on the activated complex theory (or transition theory) [35, 36] decomposition of ACN nanofibers by thermal reaction may

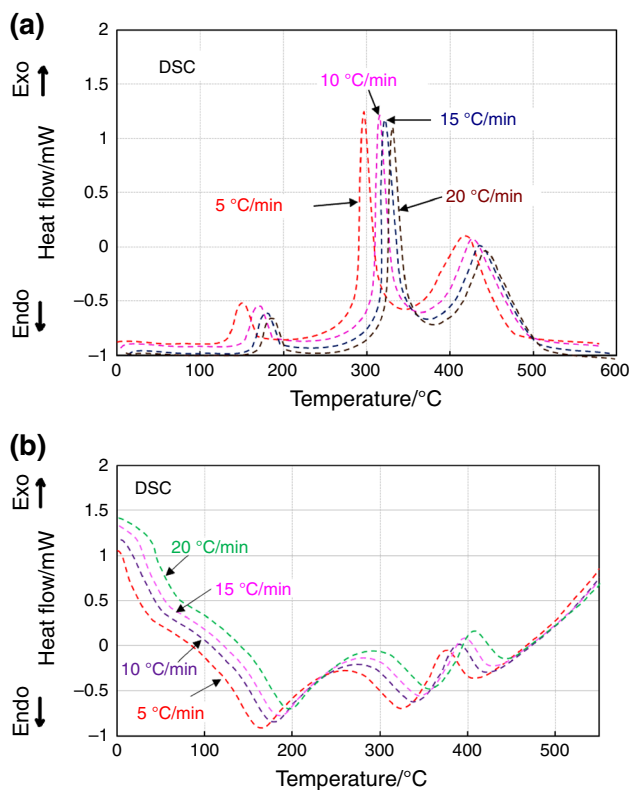


Fig. 7 The effect of heating rate on decomposition temperature of polymer nanofibers samples: **a** ACN and **b** PU; sample mass 3.0 mg; nitrogen atmosphere

Table 2 Decomposition temperature of PU and ACN nanofibers obtained by DSC at various heating rates

Heating Rate, $v_h/^\circ\text{C min}^{-1}$	Decomposition Temperature of PU nanofibers/ $^\circ\text{C}$			Decomposition Temperature of ACN nanofibers/ $^\circ\text{C}$		
	First step	Second step	Third step	First step	Second step	Third step
5	163.5	325.4	407.4	152.9	296.5	420.2
10	179.8	341.7	424.2	168.8	312.4	428.3
15	188.4	344.3	430.8	178.3	322.0	435.1
20	195.2	357.1	439.5	184.8	328.4	440.7

Table 3 Comparison of thermokinetic parameters correspond to the first step of PU and ACN nanofibers thermal decomposition obtained by ASTM and Starink methods

Sample	Method	Activation Energy/ kJ mol^{-1}	Frequency Factor Log Z/S^{-1}	Linear Regression	$\Delta G^\ddagger/\text{kJ mol}^{-1}$	$\Delta H^\ddagger/\text{kJ mol}^{-1}$	$\Delta S^\ddagger/\text{J mol}^{-1}$	LogK	$T_b/^\circ\text{C}$
PU	ASTM	66.92	7.3	0.998	115.91	63.16	-116.46	-4.40	142.2
	Starink	66.70	7.3	0.998	115.70	62.93	-116.49	-4.40	142.3
ACN	ASTM	62.8	7.02	0.999	115.1	59.0	-122	-4.00	140.7
	Starink	62.6	7.02	0.999	114.9	58.8	-122	-3.96	140.8

be interpreted as a fast reaction, while the PU nanofibers has a slow reaction rate. The positive values of ΔH^\ddagger and ΔG^\ddagger for both nanofibers showed that their reactions are dependent to the heat introducing, and these polymers are decomposed by non-spontaneous reactions. However, ΔG^\ddagger corresponds to the decomposition of PU nanofibers is slightly higher than ACN nanofibers. Furthermore, decomposition reaction of ACN nanofibers has a lower activation enthalpy (ΔH^\ddagger) in comparison with PU nanofibers.

Calculation of decomposition reaction rate constant

The decomposition reaction rate constant (k) was calculated via the following equation, while the mechanism of the decomposition reactions for the studied nanofibers was assumed as first-order reactions [37]:

$$\log k = \log Z - E_a/2.3RT. \quad (6)$$

The values of activation energies (E_a) and frequency factors (Z) obtained by ASTM and Starink methods were applied to the equation for the temperature of 25 $^\circ\text{C}$ in order to determining the decomposition reaction rates (k). Table 3 presents the values of $\log k$ for PU and ACN nanofibers. Comparison the reaction rate constants of these nanofibers show that the reaction rate constant of PU nanofibers is higher than that calculated for the ACN nanofibers. This lower reaction rate constant for ACN nanofibers confirms that these nanofibers have a considerable higher half-life rather than PU nanofibers at the identical storage conditions.

Critical ignition temperature

Another important factor for the safe storage and process operations of organic compounds is their critical ignition temperature (T_b), which is defined as the lowest temperature that the compound could be heated without undergoing thermal runaway [38–40]. This parameter for the compound based on the combustion theory could be predicted using corresponded thermokinetic parameters i.e., activation energy, pre-

exponential factor, and heat of reaction. Thus, the values of critical ignition temperature (T_b) for the PU and ACN nanofibers were computed using the following equations [38]:

$$T_e = T_{e0} + b\phi_i + c\phi_i^2, \quad i = 1 - 4, \quad (7)$$

$$T_b = \frac{E - \sqrt{E^2 - 4ERT_{e0}}}{2R}. \quad (8)$$

In the Eq. (7), b and c are coefficients, and in Eq. (8), R is the gas constant, and E is the value of activation energy obtained via thermokinetic method. The values (T_{e0}), the onset temperature (T_e) corresponding to $\phi \rightarrow 0$, were obtained by Eq. (7) as 126.6 °C and 120.2 °C for PU nanofibers and ACN nanofibers, respectively. The calculated temperatures were applied in Eq. (8) to predict the critical ignition temperatures (T_b) of PU and ACN nanofibers. Table 3 shows the obtained values of T_b for PU and ACN nanofibers.

Comparison thermal stability of nanofibers and bulk material

As shown in Fig. 5, thermal behavior of PU nanofibers is similar to the PU micron-sized particles. TG/DSC curves for the PU in the both form of nanofibers and micron-sized particles showed similarly three endothermic phenomena. However, the results showed that decomposition temperature of PU depends on its size, and decomposition temperature of PU micron-sized particles is considerably higher than its nanofibers.

On the other hand, TG and DSC curves for ACN nanofibers, and its micron-sized particles are shown in Fig. 6. ACN samples have similar thermal behaviors and exhibit three exothermic phenomena during thermal decomposition. However, the results revealed that thermal decomposition of ACN nanofibers started at 168 °C with 7 % mass loss, but decomposition of ACN micron-sized particles started at 214 °C with approximately 15 % mass loss in this step. These results reveal that decomposition temperature of ACN is also depending on the size of material, and thermal decomposition of ACN nanofibers is considerably higher than its micron-sized particles.

Comparison the obtained thermokinetic results by ASTM and Starink methods reveal that value of activation energy calculated for PU nanofibers and ACN nanofibers by starink method is slightly lower than those of ASTM method. However, the calculated values of activation energy values by ASTM and Starink method show a good agreement with each other. Meanwhile, comparing thermal stability of both nanofiber samples shows that PU nanofiber has higher decomposition activation energy. The result of thermal stability investigation on PU nanofibers and ACN nanofibers as polymer materials is valuable in usage of these compounds in future for energetic formulations, because in comparison between

thermal stability data for these energetic compounds with conventional materials, one of these energetic compounds (PU nanofibers) has considerably higher thermal stability, but another compound (ACN nanofibers) has lower activation energy for initiation of its thermal decomposition reaction.

Conclusions

Thermal decomposition of two polymers was investigated via differential scanning calorimetry (DSC) and simultaneous differential thermal analysis and thermogravimetry (TG/DSC). DSC curves of the compounds obtained under different heating rates were used for prediction kinetic and thermodynamic parameters of their thermal decomposition reactions. Meanwhile, activation energies and frequency factors for the decomposition of nanofibers of both polymers samples were calculated via different methods. Based on the TG/DSC and kinetic data obtained from decomposition reactions of both polymers, PU nanofibers, and ACN nanofibers have comparable thermal stability similar to their micron-sized particles.

References

- Shamsipur M, Pourmortazavi SM, Hajmirsadeghi SS, Atifeh SM. Effect of functional group on thermal stability of cellulose derivative energetic polymers. *Fuel*. 2012;95:394–9.
- Nagayama K, Oyumi Y. Combustion characteristics of high burn rate azide polymer propellant. *Propell Explos Pyrotech*. 1996;21:74–8.
- Barbieri U, Polacco G, Keicher T, Massimi R. Preliminary characterization of propellants based on p(GA/BAMO) and pAMMO binders. *Propell Explo Pyrotech*. 2009;34:427–35.
- Dubis C, Perreault F. Shelf-life prediction of propellants using a reaction severity index. *Propell Explos Pyrotech*. 2002;27:253–61.
- Ramesh S, Rajalingam P, Radhakrishnan G. Chain-extended polyurethanes - synthesis and characterization. *Polymer Int*. 1991;25:253–6.
- Provas A. Characterisation and polymerisation studies of energetic binder systems, DSTO-TR-1171. 2001.
- Ahmad S, Ashraf SM, Sharmin E, Zafar F, Hasant A. Studies on ambient cured PU modified epoxy coatings synthesized from sustainable resource. *Prog Cryst Growth Charact Mater*. 2002;45:83–8.
- Kendagannaswamy BK, Siddaramaiah. Chain extended polyurethane-synthesis and characterization. *J Appl Polym Sci*. 2002;84:359–69.
- Oprea S. Effects of fillers on polyurethane resin-based polyurethane elastomeric bearing materials for passive isolation. *J Comp Mater*. 2008;42:285–2673.
- Inagaki M, Yang Y, Kang F. Carbon nanofibers prepared via electrospinning. *Adv Mater*. 2012;24:2547–66.
- Persano L, Camposeo A, Tekmen C, Pisignano D. Industrial upscaling of electrospinning and applications of polymer nanofibers: a review. *Macromol Mater Eng*. 2013;298:504–20.
- Han X-J, Huang Z-M, Huang C, Du Z-F, Wang H, Wang J, He C-L, Wu Q-S. Preparation and characterization of electrospun polyurethane/inorganic-particles nanofibers. *Polym Compos*. 2012;33:2045–57.

13. Kohsari I, Pourmortazavi SM, Hajimirsadeghi SS. Non-isothermal kinetic study of the thermal decomposition of diaminoglyoxime and diaminofurazan. *J Therm Anal Cal.* 2007;89:543–6.
14. Li R, Xu H, Hu H, Yang G, Wang J, Shen J. Microstructured Al/Fe₂O₃/nitrocellulose energetic fibers realized by electrospinning. *J Energ Mater.* 2014;32:50–9.
15. Xie L, Shao Z, Wang W, Wang F. Preparation of Al-NPs/NC composite nanofibers by electrospinning. *Integr Ferroelectr.* 2011;127:184–92.
16. Azimfar F, Kohsari I, Pourmortazavi SM, investigation on decomposition kinetic and thermal stability of metallocene catalysts. *J Inorg Organomet Polym.* 2009;19:181–6.
17. Gao D, Qiao H, Wang Q, Cai Y, Wei Q. Structure, morphology and thermal stability of porous carbon nanofibers loaded with cobalt nanoparticles. *J Eng Fiber Fabr.* 2011;6:6–9.
18. Vald S. Influence of the chain extender length and diisocyanate amount on the thermal stability and mechanical properties of some polyurethanes. *Mater Plast.* 2008;45:394–7.
19. Pourmortazavi SM, Kohsari I, Teimouri MB, Hajimirsadeghi SS. Thermal behaviour kinetic study of the dihydroglyoxime and dichloroglyoxime. *Mater Lett.* 2007;61:4670–3.
20. Abu-Saied MA, Abdelrazek Khalil K, Al-Deyab SS. Preparation and characterization of poly vinyl acetate nanofiber doping copper metal. *Int J Electrochem Sci.* 2012;7:2019–27.
21. Nagle DJ, Celina M, Llewellyn R, Fredericks PM. Infrared microspectroscopic study of the thermo-oxidative degradation of hydroxyl terminated polybutadiene/isophorone diisocyanate polyurethane rubber. *Polym Degrad Stabil.* 2007;92:1446–54.
22. Chattopadhyay DK, Webster DC. Thermal stability and flame retardancy of polyurethanes. *Prog Polym Sci.* 2009;34:1068–133.
23. Bhunia HP, Jana RN, Basak A, Lenka S, Nando GB. Synthesis of polyurethane from cashew nut shell liquid (CNSL), a renewable resource. *J Polym Sci, Part A: Polym Chem.* 1998;36:391–400.
24. Vigo TL, Sachinvala N. Deoxycelluloses and related structures. *Polym Adv Technol.* 1999;10:311–20.
25. Chao JW, So JH. Polyurethane- silver fibers prepared by infiltration and reduction of silver nitrate. *Mater Lett.* 2006;60:2653–5.
26. Maeda S, Yurimoto J, Samukawa S, Kojima Y. Stabilized polyurethane. *Japan* 14, 752 (66) 1963. *C.A.* 66, 86, 263, 1967.
27. Gao H-X, Zhao F-Q, Hu R-Z, Zhao H-A, Zhang H. Estimation of the critical temperature of thermal explosion for azido-acetic acid-2-(2-azido-acetoxy)-ethylester using non-isothermal DSC. *J Therm Anal Cal.* 2009;95:477–82.
28. ASTM E698, Test methods for Arrhenius kinetic constants for thermally unstable materials.
29. Pourmortazavi SM, Hosseini SG, Rahimi-Nasrabadi M, Hajimirsadeghi SS, Momenian H. Effect of nitrate content on thermal decomposition of nitrocellulose. *J Hazard Mater.* 2009;162:1141–4.
30. Criado JM, Perez-Maqueda LA, Sanchez-Jimenez PE. Dependence of the pre-exponential factor on temperature. *J Therm Anal Cal.* 2005;82:671–5.
31. Starink MJ. The determination of activation energy from linear heating rate experiments: a comparison of the accuracy of iso-conversion methods. *Thermochim Acta.* 2003;404:163–76.
32. Shamsipur M, Pourmortazavi SM, Fathollahi M. Kinetic parameters of binary iron/oxidant pyrolants. *J Energ Mater.* 2012;30:97–106.
33. Shamsipur M, Pourmortazavi SM, Miran Beigi AA, Heydari R, Khatibi M. Thermal stability and decomposition kinetic studies of acyclovir and zidovudine drug compounds. *AAPS Pharm Sci Tech.* 2013;14:287–93.
34. Shamsipur M, Pourmortazavi SM, Hajimirsadeghi SS. Investigation on decomposition kinetics and thermal properties of copper fueled pyrotechnic compositions. *Combust Sci Tech.* 2011;183:575–87.
35. Charsley EL, Laye PG, Brown ME. *Pyrotechnics. Handbook of thermal analysis and calorimetry.* New York: Elsevier; 2003.
36. Humienik MO, Mozejko J. Thermodynamic functions of activated complexes created in thermal decomposition processes of sulphates. *Thermochim Acta.* 2000;344:73–9.
37. Pourmortazavi SM, Rahimi-Nasrabadi M, Kohsari I, Hajimirsadeghi SS. Non-isothermal kinetic studies on thermal decomposition of energetic materials. *J Therm Anal Calorim.* 2012;110:857–63.
38. Zhang TL, Hu RZ, Xie Y, Li FP. The estimation of critical temperatures of thermal explosion for energetic materials using non-isothermal DSC. *Thermochim Acta.* 1994;244:171–6.
39. Pickard JM. Critical ignition temperature. *Thermochim Acta.* 2002;392:37–40.
40. Pourmortazavi SM, Hajimirsadeghi SS, Kohsari I, Fathollahi M, Hosseini SG. Thermal decomposition of pyrotechnic mixtures containing either aluminum or magnesium powder as fuel. *Fuel.* 2008;87:244–51.